S53P4 bioactive glass scaffolds induce BMP expression and integrative bone formation in a critical-sized diaphysis defect treated with a single-staged induced membrane technique

Eriksson, E.

2021-05

Eriksson , E , Björkenheim , R , Strömberg , G , Ainola , M , Uppstu , P , Aalto-Setälä , L , Leino , V-M , Hupa , L , Pajarinen , J & Lindfors , N C 2021 , ' S53P4 bioactive glass scaffolds induce BMP expression and integrative bone formation in a critical-sized diaphysis defect treated with a single-staged induced membrane technique ' , Acta Biomaterialia , vol. 126 , pp. 463-476 . https://doi.org/10.1016/j.actbio.2021.03.035

http://hdl.handle.net/10138/330681
https://doi.org/10.1016/j.actbio.2021.03.035

Acta Biomaterialia 126 (2021) 463–476

Contents lists available at ScienceDirect

Acta Biomaterialia

journal homepage: www.elsevier.com/locate/actbio

Full length article

S53P4 bioactive glass scaffolds induce BMP expression and integrative bone formation in a critical-sized diaphysis defect treated with a single-staged induced membrane technique

E. Eriksson[a,*], R. Björkenheim[b], G. Strömberg[b], M. Ainola[c], P. Uppstu[d], L. Aalto-Setälä[e], V-M. Leino[g], L. Hupa[e], J. Pajarinen[b,f], N.C. Lindfors[a,b]

[a] Faculty of Medicine, University of Helsinki, Helsinki, Finland
[b] Department of Musculoskeletal and Plastic Surgery, University of Helsinki and Helsinki University Hospital, Helsinki, Finland
[c] Translational Immunology Research Program, Faculty of Medicine, University of Helsinki, Helsinki, Finland
[d] Polymer Technology Research Group, Faculty of Science and Engineering, Åbo Akademi University, Turku, Finland
[e] Johan Gadolin Process Chemistry Centre, Åbo Akademi University, Turku, Finland
[f] Päijät-Häme Central Hospital, Department of Surgery, Lahti, Finland
[g] Department of Physics, University of Helsinki, Helsinki, Finland

ARTICLE INFO

Article history:
Received 6 January 2021
Revised 25 February 2021
Accepted 17 March 2021
Available online 25 March 2021

Keywords:
S53P4 bioactive glass
Scaffold for bone regeneration
Bone morphogenic proteins
Induced membrane
Critical-sized diaphysis defect
Bone substitute

ABSTRACT

Critical-sized diaphysis defects are complicated by inherent sub-optimal healing conditions. The two-staged induced membrane technique has been used to treat these challenging defects since the 1980's. It involves temporary implantation of a membrane-inducing spacer and subsequent bone graft defect filling. A single-staged, graft-independent technique would reduce both socio-economic costs and patient morbidity. Our aim was to enable such single-staged approach through development of a strong bioactive glass scaffold that could replace both the spacer and the graft filling. We constructed amorphous porous scaffolds of the clinically used bioactive glass S53P4 and evaluated them *in vivo* using a critical-sized defect model in the weight-bearing femur diaphysis of New Zealand White rabbits. S53P4 scaffolds and standard polymethylmethacrylate spacers were implanted for 2, 4, and 8 weeks. Induced membranes were confirmed histologically, and their osteostimulative activity was evaluated through RT-qPCR of bone morphogenic protein 2, 4, and 7 (BMPs). Bone formation and osseointegration were examined using histology, scanning electron microscopy, energy-dispersive X-ray analysis, and micro-computed tomography imaging. Scaffold integration, defect union and osteosynthesis were assessed manually and with X-ray projections. We demonstrated that S53P4 scaffolds induce osteostimulative membranes and produce osseointegrative new bone formation throughout the scaffolds. We also demonstrated successful stable scaffold integration with early defect union at 8 weeks postoperative in critical-sized segmental diaphyseal defects with implanted sintered amorphous S53P4 scaffolds. This study presents important considerations for future research and the potential of the S53P4 bioactive glass as a bone substitute in large diaphyseal defects.

Statement of significance

Surgical management of critical-sized diaphyseal defects involves multiple challenges, and up to 10% result in delayed or non-union. The two-staged induced membrane technique is successfully used to treat these defects, but it is limited by the need of several procedures and bone graft. Repeated procedures increase costs and morbidity, while grafts are subject to donor-site complications and scarce availability. To transform this two-staged technique into one graft-independent procedure, we developed amorphous porous scaffolds sintered from the clinically used bioactive glass S53P4. This work constitutes the first evaluation of such scaffolds *in vivo* in a critical-sized diaphyseal defect in the weight-bearing rabbit femur. We provide important knowledge and prospects for future development of sintered S53P4 scaffolds as a bone substitute.

https://doi.org/10.1016/j.actbio.2021.03.035

1. Introduction

Historically, large bone defects often had only one, life-changing, solution: amputation [1]. Fortunately, modern-day clinicians can utilize the body's natural bone healing capacity using well-formulated principles. A well-known set of such principles is the 'diamond concept' and its revision titled the "hexagon of bone healing", according to which successful fracture healing requires inflammatory cells and mediators, growth factors, osteogenic stem cells, an osteoconductive scaffold, a mechanically stable environment, and vascularity [2,3]. Yet, natural healing is highly dependent on fracture size and location, with critical-sized diaphyseal defects still posing a major challenge for surgeons and patients.

'Critical-sized' defects generally do not heal spontaneously with surgical stabilization and require further intervention, regardless of etiology [4]. In these defects, the natural healing process is undermined by extensive bone loss, defect displacement causing vascular disruption, high demand for mechanical stability due to functional loading, and the inherently inferior healing conditions in the diaphysis [5,6]. Consequently, up to 10% result in delayed unions or non-unions [7].

In the 1980s, Alain Masquelet developed a two-staged induced membrane (IM) technique to treat these challenging defects [8]. This commonly used method involves two procedures. First, the defect is debrided and a polymethylmethacrylate (PMMA) spacer is implanted to elicit a foreign body-derived reaction resulting in a bioactive IM. This defect-enclosing IM is then carefully incisioned 4–8 weeks later, the spacer is removed, and the IM is filled with bone graft [9–12].

In the IM technique, the role of the temporary PMMA spacer is to produce the IM. PMMA is not a bone substitute and will not be replaced by new bone. Thus, the PMMA spacer needs to be removed before the bone graft can be placed in the IM to act as a scaffold for bone ingrowth and heal the defect [13]. The IM prevents graft resorption and optimizes the local healing conditions by providing stability and vascularity. It also provides stem cells and osteogenic growth factors, such as bone morphogenic proteins (BMPs) [14,15]. Notably, BMP-2 is important in osteogenic differentiation of mesenchymal progenitor cells and initiation of the fracture healing cascade, while BMP-4 and BMP-7 are key stimulators of osteoblasts and callus formation [16,17].

This utilization of the body's own signaling systems is one of the core benefits of the IM technique as it bypasses problems related to dosage, release patterns and adverse effects, which limits many manufactured drug delivery-systems [18]. The IM has been described as the ideal 'biological chamber' for the 'diamond concept' as it gathers its fracture-healing components [19], and several clinical studies have found this approach suitable for large defects in long bones [20–22].

However, the IM technique is limited by its two-staged nature and graft-dependence. Repeated surgeries infer higher socioeconomic costs and expose patients to prolonged hospitalization and morbidity. Autografts, while being the graft gold standard, are limited by donor-site complications and scarce availability – especially so in large defects [23]. We hypothesised that a mechanically stable scaffold crafted from an osteostimulative and osteoconductive bone substitute that can induce an active IM and integrate in the defect would be a promising solution to both problems.

Consequently, we developed a scaffold aimed to enable a graft-independent single-staged IM technique for the treatment of critical-sized diaphyseal defects. This amorphous porous scaffold is sintered from the bioactive glass S53P4 (BAG-S53P4). Hench and Paschall [24,25] introduced BAG in the 1960s, and it has received vast interest as a bone graft substitute. Despite being a silica-based material, it can bond firmly to living tissue in the body. Upon implantation, this bonding is initiated through a rapid exchange of Na^+ ions in the BAG with H^+ and H_3O^+ ions in body fluids, resulting in a silica-rich reaction surface on the BAG. This surface then attracts calcium and phosphate which precipitates into calcium phosphate (CaP) and crystallizes into hydroxyapatite. As hydroxyapatite resembles the natural bone mineral, it forms strong bonds with bone apatite. This surface transformation makes BAG osteoconductive and osseointegrative [26,27]. Furthermore, BAG's osteostimulative dissolution products promote osteoprogenitor cell maturation and gene expressions vital in osteogenesis and angiogenesis [28,29].

S53P4 is a BAG with non-antibiotic antimicrobial traits [30,31]. Its granular form has been clinically used since the 1990s, with successful application in chronic osteomyelitis, trauma, and bone tumours [32–34]. Utilization of BAG-S53P4 in the IM technique is a promising concept. Recently, Tanner et al. [35] initiated a clinical trial evaluating loose BAG-S53P4 granules as a bone graft replacement in large tibial and femoral defects treated with the two-staged IM technique. Still, this trial only addressed the graft-dependence and did not aim to eliminate the need of repeated surgeries. The initial PMMA spacer implantation is still needed.

Previous research on a single-staged IM technique shows that sintered non-amorphous BAG-S53P4 scaffolds implanted in mechanically stable, non-critical metaphyseal defects in New Zealand White rabbits produce new bone and IMs expressing osteogenic and angiogenic growth factors [36,37]. However, the IM technique is mainly used to treat critical-sized diaphyseal defects, which are more complex [8–12]. These unstable defects need surgical fixation and do not provide a protecting scaffold-enclosure, as the drilled-out metaphyseal defects did. Thus, bone-substituting scaffolds used in critical-sized diaphyseal defects must be strong and resistant. It has been considered difficult to sinter BAGs into strong scaffolds, but recent years has brought a greater understanding of how to reduce the brittleness of the glass through sintering optimization [38].

This preclinical study was designed to test our hypothesis. We evaluated amorphous porous BAG-S53P4 scaffolds *in vivo* using a single-staged IM technique to treat critical-sized segmental defects in the femur diaphysis of New Zealand White rabbits. We studied the scaffold's capability to (1) form IMs similar to those induced by standard PMMA spacers, (2) promote osteogenesis through IM expressions of key BMPs in comparison with the expressions in PMMA IMs, and (3) achieve stable scaffold integration through osseointegrative new bone formation with successful osteosynthesis and early defect union.

2. Material and methods

2.1. Materials

2.1.1. Bioactive glass S53P4 scaffolds

We used BAG-S53P4 granules of size fraction 315–500 µm (Bonalive Biomaterials, Turku, Finland) to develop amorphous scaffolds robust enough for application in large weight-bearing long bone defects. The wt. % composition of BAG-S53P4 is 53% SiO_2, 23% Na_2O, 20% CaO, 4% P_2O_5, and its density is 2.66 kg/dm^3 [39]. The granules were sintered using pressureless sintering into cylindrical shapes under carefully controlled conditions in uncovered graphite molds at 630 °C for 60 min in a nitrogen atmosphere in a tubular oven. The amorphous porous BAG-S53P4 scaffolds (Fig. 1) measured 10 mm × 10 mm with an average mass of 831 mg. The scaffold porosity was 50.0 ± 3.0% and the compressive strength of dry

* Corresponding author at: University of Helsinki, Helsinki University Hospital, C/o Nina Lindfors, Topeliuksenkatu 5B, 00260 Helsinki, Finland.
E-mail address: elin.eriksson@helsinki.fi (E. Eriksson).

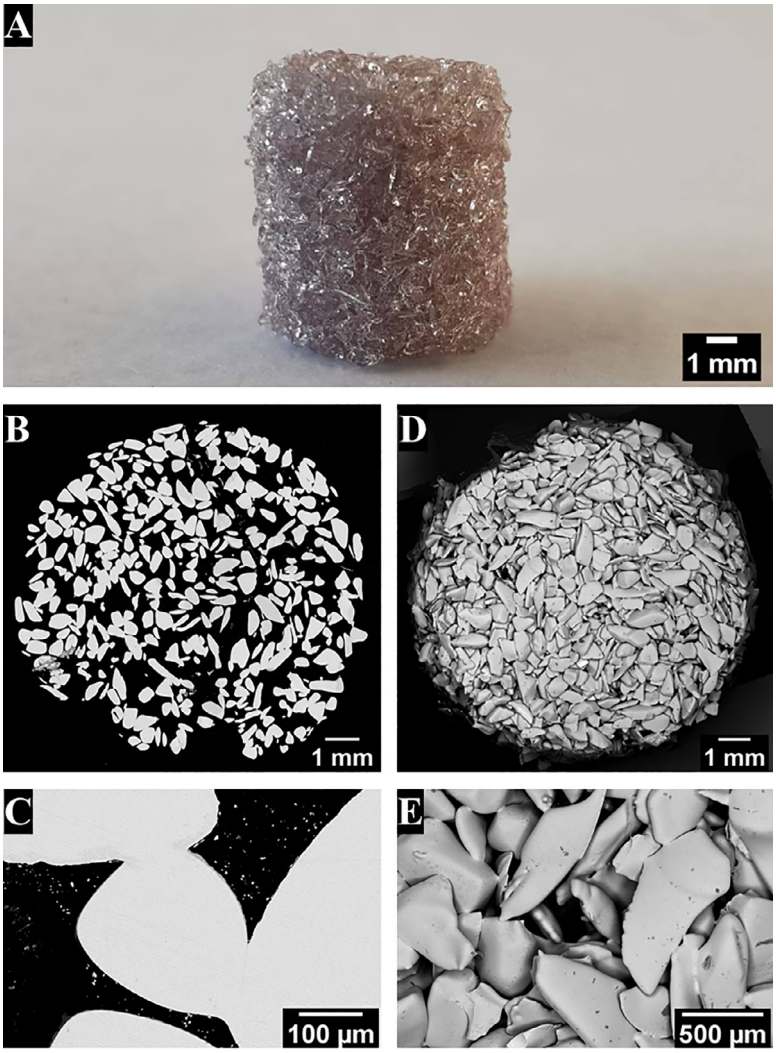

Fig. 1. Images depicting the macroscopic and microscopic structure of the realized sintered BAG-S53P4 scaffolds pre-implantation. A: Representative photo of a 10 mm × 10 mm BAG-S53P4 scaffold. B–C: SEM backscattered electron images of a BAG-S53P4 scaffold cut in the transversal plane, without magnification (B) and with 200× magnification (C). D–E: SEM backscattered electron images of the outer top surface of a BAG-S53P4 scaffold, without magnification (D) and with 50× magnification (E).

scaffolds was 4.80 ± 0.60 MPa (mean ± standard error of the mean (SEM)) [40]. Compared to porous BAG-S53P4 scaffolds described in earlier literature, the strength of our scaffolds are 10 times higher [41] and corresponds to the values (2–10 MPa) reported for trabecular bone [42]. Measurement through micro-computed tomography of a BAG-S53P4 scaffold with a porosity of 49.8% rendered a mean pore size of 0.19 ± 0.07 mm (mean ± standard deviation), with a maximum pore size of 0.51 mm, and a mean neck diameter of 0.23±0.18 mm. Scaffolds were sterilized using gamma irradiation with a dose of 25 kGy.

2.1.2. Standard polymethylmethacrylate spacers

Cylindrical, non-porous (compact) PMMA (Palacos R+G, Heraeus Medical GmbH, Wehrheim, Germany) spacers of 10 mm × 10 mm in size were constructed under sterile conditions according to the manufacturer's instructions and sterilized in an autoclave prior to implantation.

2.2. In vivo *experimental animal model*

All protocols were approved by the National Animal Experimental Board of Finland (permit number: ESAVI/6423/04.10.07/2017) and conducted in compliance with the principles established at the University of Helsinki, the ARRIVE guidelines, and the Directive 2010/63/EU of the European Parliament and the Council of the European Union.

A critical-sized, weight-bearing diaphyseal defect model was designed using 18 female New Zealand White (NZW) rabbits (Harlan laboratories, The Netherlands) in three parallel experiments with study endpoints at 2, 4, and 8 weeks. Each experiment included an experimental BAG-S53P4 scaffold group ($n = 3$) and a standard PMMA spacer group ($n = 3$). In total, BAG-S53P4 scaffolds and PMMA spacers were allocated to nine rabbits each ($n = 9$ for each). At study initiation, the rabbits were skeletally mature (aged 10–11 months) with body weights (mean ± SEM) of 3.3 ± 0.1 kg (BAG-S53P4 groups) and 3.6 ± 0.1 kg (PMMA groups). Allocation to the parallel experiments was made according to the supplier-provided rabbit identification numbers. Scaffolds were allocated using a computer-based random number generator and block randomization. Animal care staff were blinded to allocation, but investigators were not blinded.

The implantation procedures were initiated using medetomidine hydrochloride (Cepetor, 0.5 mg/kg s.c.) and ketamine hydrochloride (Ketalar, 25 mg/kg s.c.) to put the non-fasting animals under general anesthesia in their cages to minimize stress. Preoperative buprenorphine (Vetergesic, 0.05 mg/kg s.c. ×1), cefuroxime

(Zinacef, 40 mg/kg s.c. ×1), and carprofen (Rimadyl, 4 mg/kg s.c. ×1) was administered to prevent pain and infection. The femoral area was shaved, and animals were placed in standard decubitus position in the semi-sterile operation room. A lateral approach exposed the femur using standard sterile procedures. A 1 cm long segment of the mid-diaphysis was removed with a surgical saw, and the defect gap was filled with a BAG-S53P4 scaffold or a PMMA spacer. The 1 cm defect size corresponds to 100% of the femur circumference and has been verified not to heal spontaneously [43–45]. A rigid fixation of the femur was achieved using a 59 mm long 8-hole locking compression plate (Veterinary Instrumentation, Sheffield, United Kingdom). The plate was placed on the femur over the BAG-S53P4 scaffold or the PMMA spacer and attached to the bone with three 2.4-mm screws on each side of the implant. A 1 mm stainless-steel wire was then placed around the implant and the plate to prevent implant displacement. Sutures closed the wound. Perioperative corneal drying and heat loss were prevented with ophthalmic ointment and heating pads, respectively. After implantation, the preoperative buprenorphine and cefuroxime administration was repeated.

Postoperatively, Cefuroxime (Zinacef, 40 mg/kg s.c. ×3), buprenorphine (Vetergesic, 0.01 mg/kg s.c. ×2), and carprofen (Rimadyl, 4 mg/kg s.c. ×1) were given for three days to provide analgesia and prevent infection. The animals had free mobility in their cages and were monitored closely by skilled animal care staff. To secure humane endpoints, animals showing signs of pre- or postoperative complications were switched to an earlier study endpoint without any further result assessment or were excluded from the study. Two rabbits in the overall PMMA group were switched with rabbits at earlier endpoints due to postoperative wound infection. One rabbit in the 2-week PMMA group was excluded due to unexplained preoperative vaginal bleed. Hence, $n = 8$ for that group. The study included 17 rabbits post exclusion.

At 2, 4, and 8 weeks postoperative, corresponding animals were put under general anesthesia in their cages using the already described method and euthanized using a pentobarbital overdose (Mebunat Vet, 60 mg/kg i.p. ×1). Femurs, implants, and surrounding membranes were collected. Samples for histochemical analysis and imaging were stored in 10% formalin overnight, washed, and stored in 70% EtOH. Samples for RT-qPCR analysis were stored in RNA later solution (Invitrogen, USA) in +4°C overnight and then stored in sterile tubes in −80 °C.

2.3. Histology

2.3.1. Hematoxylin and eosin staining

Tissue samples of IMs from BAG-S53P4 scaffolds and PMMA spacers were stained with hematoxylin and eosin (H&E) and histologically examined. Samples were prepared using a KOS multifunctional microwave tissue processor (Milestone Srl, Sorisole BG, Italy) and embedded in paraffin blocks using a Microm EC 350 Tissue Embedding Center (Thermo Scientific, MI, USA). A Motorized Rotary Microtome Leica RM2255 (Leica Microsystems, Wetzlar, Germany) cut the blocks into 3-µm sections, which were then deparaffinized in xylene and hydrated to water in a descending alcohol series using a Varistain XY robotic slide stainer (Thermo Scientific, Cheshire, England). A 10-min incubation in hematoxylin stained cell nuclei, and a 5-min incubation in eosin stained cytoplasm and extracellular matrix. Stained sections were dehydrated in an ascending alcohol series, cleared by immersion in xylene, mounted, and analysed using a Leica DM6000 B/M light microscope with a digital camera (Leica Microsystems, Wetzlar, Germany).

2.3.2. Goldner's Masson trichrome staining

Resected femurs with implanted BAG-S53P4 scaffolds were transversally cut with a diamond saw, stained with Goldner's Masson trichrome stain, and examined. Cut segments were processed and stained at BioSiteHisto Ltd. (Helsinki, Finland). Images were generated using 3DHISTECH Pannoramic 250 FLASH II digital slide scanner at Genome Biology Unit supported by HiLIFE and the Faculty of Medicine, University of Helsinki, and Biocenter Finland. Histopatohological changes were assessed by a professional pathologist at the Finnish Centre for Laboratory Animal Pathology (Department of Veterinary Biosciences, University of Helsinki, Finland).

Table 1
Primer sequences used in RT-qPCR analysis of relative gene expressions in tissue samples from induced membranes of BAG-S53P4 scaffolds and PMMA spacers.

Gene	Primer	Primer sequence (5′–3′)	Bp.	Acc. No.
GAPDH	Forward Reverse	TGGTGAAGGTCGGAGTGAAC GGCGACAACATCCACTTTGC	89	NM_001082253
BMP-2	Forward Reverse	CAGCGGAAACGCCTCAAATC ACACAGCATGCCTTCGGAAT	224	NM_001082650
BMP-4	Forward Reverse	TGAGGAGCTTCCACCACGAA ATGGCCTCGTTCTCTGGGAT	109	NM_001195723
BMP-7	Forward Reverse	AACTGTACGTCAGCTTCCGC GGTGGCGTTCATGTAGGAGT	122	XM_008253604

2.4. Real-time quantitative polymerase chain reaction analysis

Relative gene expressions in IMs from BAG-S53P4 scaffolds and PMMA spacers were analyzed using real-time quantitative polymerase chain reaction (RT-qPCR). IM tissue samples of 30–50 mg were homogenized (speed 6.5, 2 × 20 s) in 300 ml RLT^{+} buffer solution with 10 µl β-mercaptoethanol (Bio-Rad/Life Science Research, USA) per 1 ml buffer using a FastPrep-24^{TM} Homogenizer (MP Biomedicals, USA) and Precellys Lysing Kit CK28 (Bertin Instruments, France). Liquid phase with total RNA was pretreated with 10 µl Proteinase K (Qiagen, CA, USA) in 590 µl RNase free water and isolated using RNeasy Plus Mini Kit (Qiagen, CA, USA). A NanoDrop 1000 spectrophotometer (Thermo Scientific, Wilmington, DE) was used to measure total RNA, and its integrity was assessed using denaturing agarose gel analysis with Ethidium Bromide (Amresco, Solon, OH) staining. Isolated RNA (2000 ng per sample) was reverse transcribed into cDNA using iScript^{TM} cDNA synthesis kit (Bio-Rad, CA, USA) and diluted 1:5 with RNase-free water. A LightCycler96 real-time PCR System (Roche, Basel, Switzerland) was used to perform RT-qPCR in duplicate wells with a reaction mixture containing iQ^{TM} SYBR® Green supermix reagent (Bio-Rad/Life Science Research), 20 ng sample cDNA, and primer pair mix (Table 1). Negative controls contained RNase-free water instead of cDNA. The housekeeping gene Glyceraldehyde-3-Phosphate Dehydrogenase (GAPDH) was used for relative quantification. Relative gene expressions were calculated from RT-qPCR results using the Gene Expression Macro (Bio-Rad/Life Science Research, version 1.1) and the comparative Ct method [46].

2.5. Manual assessment and X-ray imaging

Segmental defects with implanted BAG-S53P4 scaffolds were assessed manually in situ and after femur resections at 2, 4, and 8 weeks to evaluate achieved scaffold integration, state of the osteosynthesis, and signs of early defect union. Manual assessments were supplemented by X-ray imaging (Phoenix Xray Systems & Services GmbH, Germany) of resected femurs. Each defect with an implanted BAG-S53P4 scaffold was qualitatively assessed as 'Full integration', 'Partial integration', or 'Not integrated'. Samples assessed as 'Full integration' presented a stably integrated BAG-S53P4 scaffold, a successful osteosynthesis with sufficient alignment and signs of early union in both defect ends, in situ as well as after resection. Samples assessed as 'Partial integration' fulfilled the 'Full

integration' criteria in only one defect end or presented scaffold dislocation, but not detachment, during or after resection. In 'Not integrated' samples, the scaffolds detached completely during or after resection.

2.6. Scanning electron microscopy imaging and energy-dispersive X-ray analysis

Resected femurs with implanted BAG-S53P4 scaffolds were transversally cut into 3 mm thick discs using a diamond saw and subject to scanning electron microscopy (SEM) and energy-dispersive X-ray analysis (EDXA). Discs cut from the longitudinal end area of the implanted scaffolds were cast in epoxy resin, ground, and polished. Panoramic cross-sectional SEM images were taken with a LEO 1530 Gemini SEM instrument (Carl Zeiss, Oberkochen, Germany) with an acceleration voltage of 20 kV at up to 75× magnification using Polaroid 545 as reference. The quad back scatter detector was in Composition mode and with BSD Gain adjusted to 'high'. EDXA (UltraDry Silicon Drift Detector, Thermo Scientific, Wisconsin, US) enabled elemental identification of reaction surface layers inside the BAG-S53P4 scaffolds. Two 2-week and one 4-week scaffold were excluded from SEM and EDXA due to detachment during femur resection, which compromised the sample cutting process.

2.7. Micro-computed tomography imaging and ImageJ area measurement

Micro-computed tomography imaging (µCT) scans of resected femurs and BAG-S53P4 scaffolds were obtained using a Nanotom 180 NF apparatus (Phoenix X-Ray Systems & Services GmbH, Germany) with 15 µm image resolution. Image artifacts from metallic fixation were effectively removed with a threshold adapted binary mask and background subtraction utilizing the Rolling Ball-algorithm with a radius of approximately 1.50 mm (ImageJ, version 1.52p). Transversal series of µCT images, approximately 0.25 to 0.45 mm apart, were created from each scan. The µCT images were sectioned according to their placement in the scaffold ends or middle, with each section representing 33% (3.3 mm in length) of the whole scaffold. End sections were grouped together in subsequent analysis as the proximal/distal orientation could not always be reliably determined.

Areas corresponding to the whole BAG-S53P4 scaffold, remaining BAG-S53P4, and formed reaction surface and new bone inside the scaffold were measured by thresholding for applicable grey values in the µCT images using ImageJ software (version 1.53d). Secure thresholding separation of reaction surface and new bone could not be established, and these areas were therefore measured together. Tissue external to the implanted scaffold, such as formed callus and diaphysis ends, were excluded to only measure areas inside the BAG-S53P4 scaffolds. Area measurements were completed by one author (E.E.) at two different time points and the resulting average values were used for statistical analysis.

2.8. Statistical analysis

Statistical analyses were performed using Prism software (GraphPad Software, Inc., version 8.0.0). Relative gene expressions in IMs of BAG-S53P4 scaffolds and PMMA spacers, and µCT image area measurements of BAG-S53P4 scaffolds were analyzed using one-way ANOVA [47] followed by Tukey's post hoc test [48] for comparison of the implant types at 2, 4, and 8 weeks. Unpaired *t*-tests [47] were used to compare relative gene expressions in BAG-S53P4 IMs with PMMA IMs. Nonparametric Mann–Whitney *U* tests [48] were used to compare µCT image area measurements in the end and middle sections of BAG-S53P4 scaffolds. Underlying assumptions of data normality and equality for ANOVA and *t*-tests were evaluated with Q-Q-plots and F-tests [49]. The threshold of statistical significance was $p < 0.05$. Results are presented as mean ± SEM.

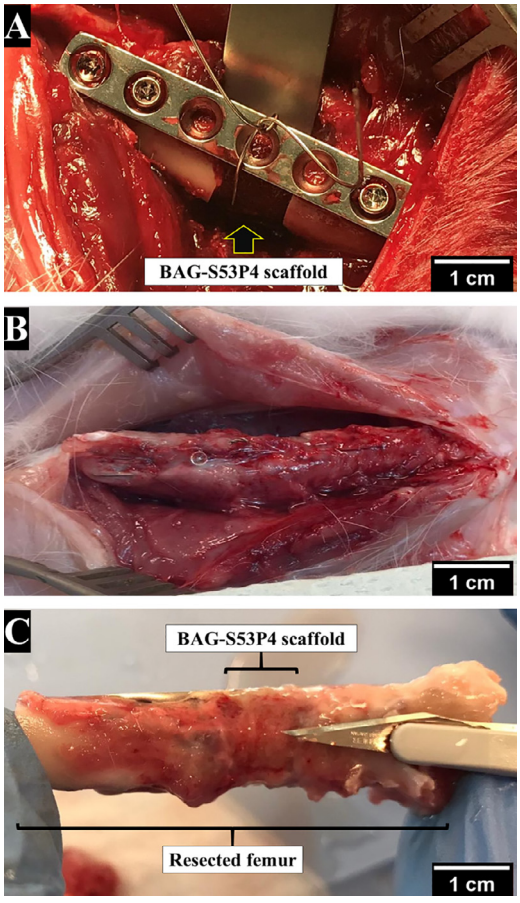

Fig. 2. Representative overview of the intra-operative process. Photos taken of a BAG-S53P4 scaffold (A) during implantation in the segmental defect created in the mid-shaft of a rabbit femur, (B) in situ prior to femur resection at 8 weeks postoperative, and (C) in the resected femur at 8 weeks postoperative. An induced membrane can be seen enclosing the well-aligned defect and the integrated BAG-S53P4 scaffold in photo C.

3. Results

3.1. Histological assessment of induced membranes

3.1.1. BAG-S53P4 scaffolds form induced membranes around critical-sized diaphyseal defects

During the sample collection procedures at 2, 4, and 8 weeks postoperative, we found that defect-enclosing IMs had formed in all femur samples with implanted BAG-S53P4 scaffolds (Fig. 2) or PMMA spacers. Analysis of H&E-stained tissue samples confirmed that IMs of BAG-S53P4 and PMMA were structurally similar and formed a distinct interface adjacent to the implant (Fig. 3).

3.2. RT-qPCR and analysis of relative gene expressions in induced membranes

3.2.1. Expressions of BMP-2, -4, and -7 are upregulated in membranes induced by BAG-S53P4

RT-qPCR confirmed upregulated expressions of BMP-2, -4, and -7 in IMs of both BAG-S53P4 scaffolds and PMMA spacers at 2, 4, and 8 weeks, but the expression patterns differed (Fig. 4).

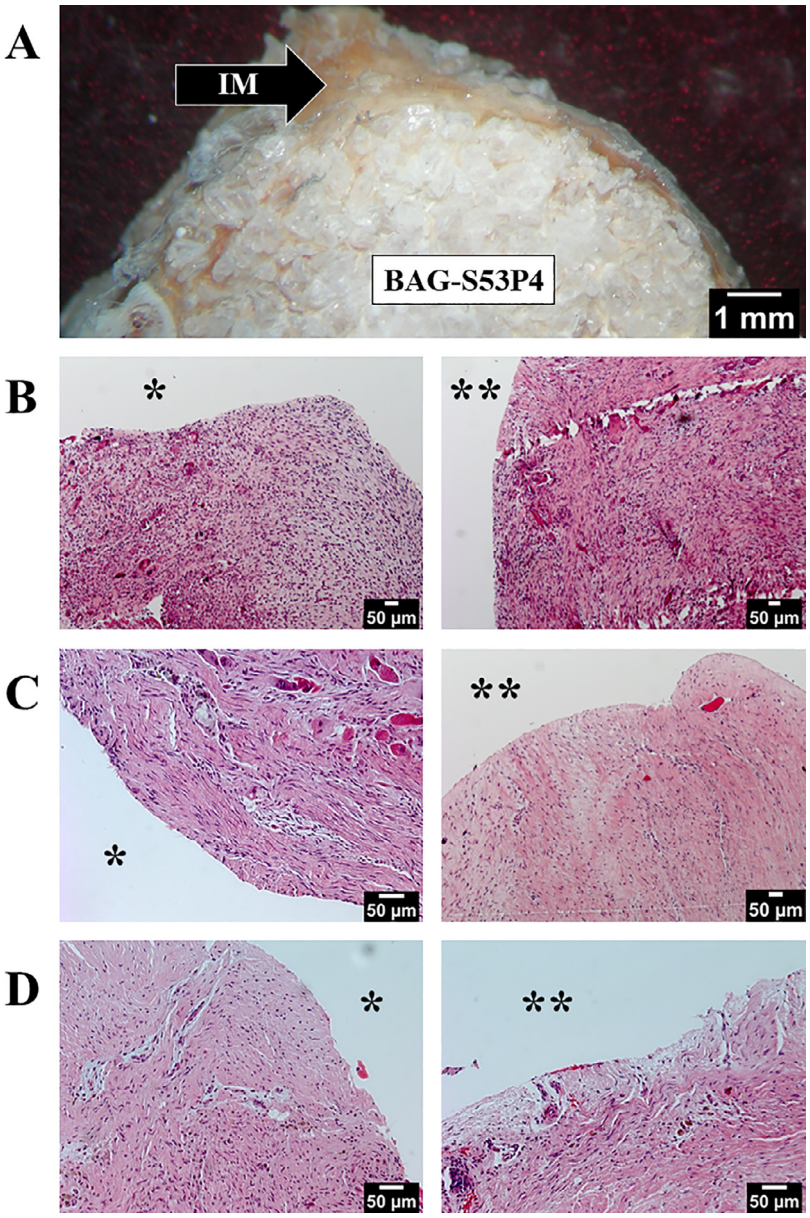

Fig. 3. Membranes induced by BAG-S53P4 scaffolds and PMMA spacers. A: Photo showing a representative induced membrane (IM, indicated by a black arrow) formed around an 8-week BAG-S53P4 scaffold cut in the transversal plane in the longitudinal end region of the scaffold after femur resection. B–D: Representative H&E-stained tissue samples from induced membranes formed around PMMA spacers (left) and BAG-S53P4 scaffolds (right) at 2 (B), 4 (C), and 8 weeks (D). A single asterisk (*) indicates the interface against PMMA, and double asterisks (**) indicates the interface against BAG-S53P4.

BMP-2 expression in BAG-S53P4 IMs peaked at 2 weeks and then decreased evenly throughout 4 and 8 weeks. In contrast, BMP-2 in PMMA IMs increased from a low expression at 2 weeks and peaked at week 4 and 8. The only significant difference was at 8 weeks, when PMMA IMs presented higher BMP-2 expression than BAG-S53P4 IMs (3.8 ± 0.6 *vs.* 1.2 ± 0.7, $p = 0.045$).

BMP-4 expression in BAG-S53P4 IMs was persistently upregulated at 2 and 4 weeks and showed no distinct decrease until week 8. In PMMA IMs, BMP-4 expression increased significantly from 2 to 4 weeks (2.0 ± 0.5 vs 4.9 ± 0.6, $p = 0.021$), peaked at 4 weeks, and then decreased during week 4 to 8 (4.9 ± 0.6 vs 2.8 ± 0.3, $p = 0.045$). At 8 weeks, the expression of BMP-4 was significantly higher in PMMA IMs compared with BAG-S53P4 IMs (2.8 ± 0.3 vs. 0.5 ± 0.1, $p = 0.001$).

Expression of BMP-7 in BAG-S53P4 IMs was high at 2 and 4 weeks and then decreased to a low expression at 8 weeks. In PMMA IMs, BMP-7 expression was low at 2 weeks, peaked at 4 weeks, and persisted at 8 weeks. At 2 weeks postoperative, BAG-S53P4 IMs had a significantly higher BMP-7 expression compared with PMMA IMs (3.4 ± 0.7 vs. 0.2 ± 0.1, $p = 0.036$).

3.3. Manual assessment and X-ray imaging of defects with BAG-S53P4 scaffolds

3.3.1. Critical-sized diaphyseal defects with implanted BAG-S53P4 scaffolds can achieve stable scaffold integration and early defect union

Results of combined manual and X-ray assessments of the segmental defects with implanted BAG-S53P4 scaffolds are presented in Table 2. Results at 2 and 4 weeks were heterogeneous, while all 8-week scaffolds were markedly integrated, and all 8-week defects demonstrated successful osteosynthesis and signs of early union. Fig. 5 presents X-ray projections of femur samples demonstrating a 'Partial integration' at 2 weeks, the 'Full integration' at 4 weeks, and one representative 'Full integration' at 8 weeks postoperative. The 2-week 'Partial integration' was stable during resection, but

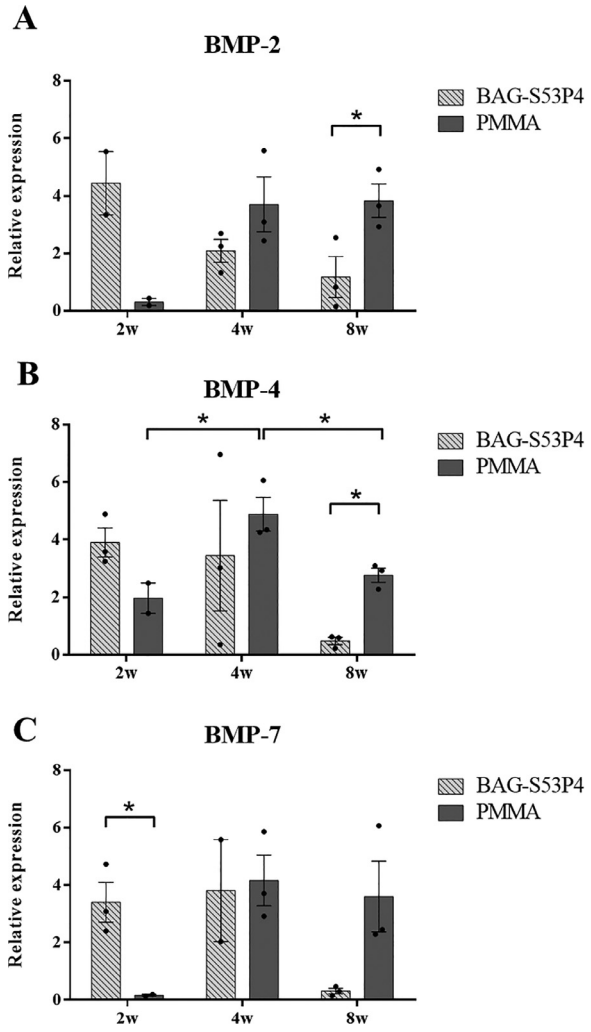

Fig. 4. Relative gene expressions of BMP-2 (A), BMP-4 (B), and BMP-7 (C) in induced membranes. Bars show mean ± SEM. Mean relative gene expressions in induced membranes formed around BAG-S53P4 scaffolds and PMMA spacers are compared at 2, 4, and 8 weeks postoperative, and a single asterisk (*) indicates differences for which $p < 0.05$.

Table 2
Summarized results of combined manual and X-ray assessments of segmental defects with implanted BAG-S53P4 scaffolds. Qualitative evaluation of achieved scaffold integration, state of the osteosynthesis, and defect alignment as well as signs of early defect union at 2, 4, and 8 weeks postoperative.

	Study endpoints		
Assessment	2 weeks ($n = 3$)	4 weeks ($n = 3$)	8 weeks ($n = 3$)
Not integrated	2	1	-
Partial integration	1	1	-
Full integration	-	1	3

later dislocated partially during sample transport. The 4- and 8-week samples assessed as 'Full integration' showed no scaffold dislocation and continued to present stability and alignment during postoperative handling.

3.4. SEM imaging and EDXA of BAG-S53P4 scaffolds

3.4.1. BAG-S53P4 scaffolds show internal new bone formation and external osseointegration

SEM imaging demonstrated progressive formation of reaction surface and new bone inside the BAG-S53P4 scaffolds and osseointegration of the scaffolds in surrounding callus (Fig. 6). Modest

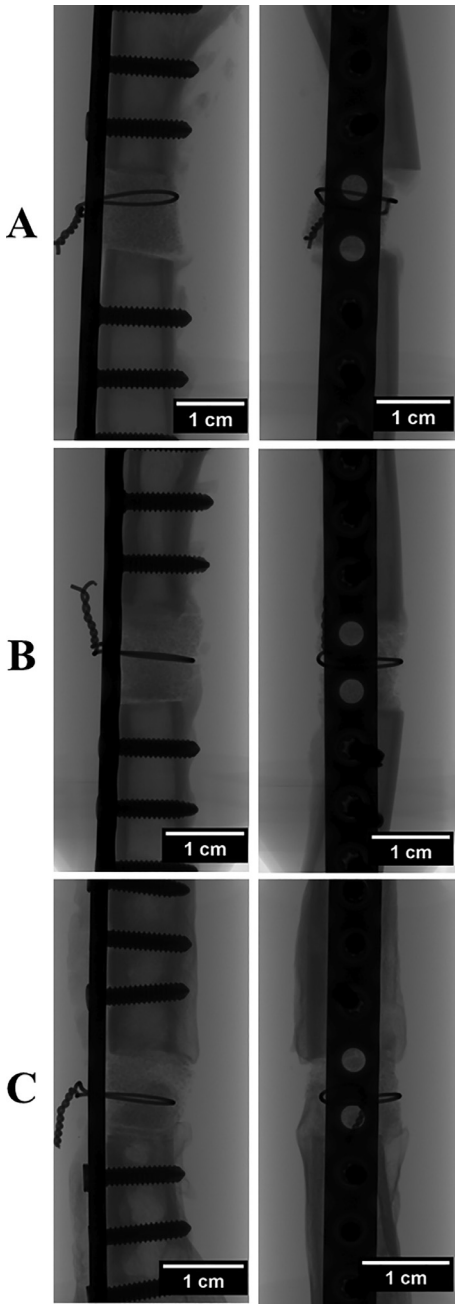

Fig. 5. X-ray projections in two directions of segmental defects with implanted BAG-S53P4 scaffolds at 2 (A), 4 (B), and 8 (C) weeks postoperative. The resected femur samples are oriented with the proximal femur end positioned at the top of the image, and the distal end at the bottom.

new bone formation was present already at 2 weeks postoperative but was notably more pronounced at 4 weeks. At 8 weeks, considerable new bone formation and trabecular intergrowth of scaffold and surrounding callus, namely osseointegration, had developed.

3.4.2. Bone-bonding calcium phosphate precipitate on BAG-S53P4 in the scaffolds

EDXA confirmed the composition of the reaction surface formed on the BAG-S53P4 and the formation of new bone in the porous spaces inside the scaffolds, as observed in SEM imaging (Fig. 7). The reaction surface can be described as a compositional continuum, with a region rich in Si closest to still remaining glass, and an outer region of CaP effectively bridging the Si-layer to new

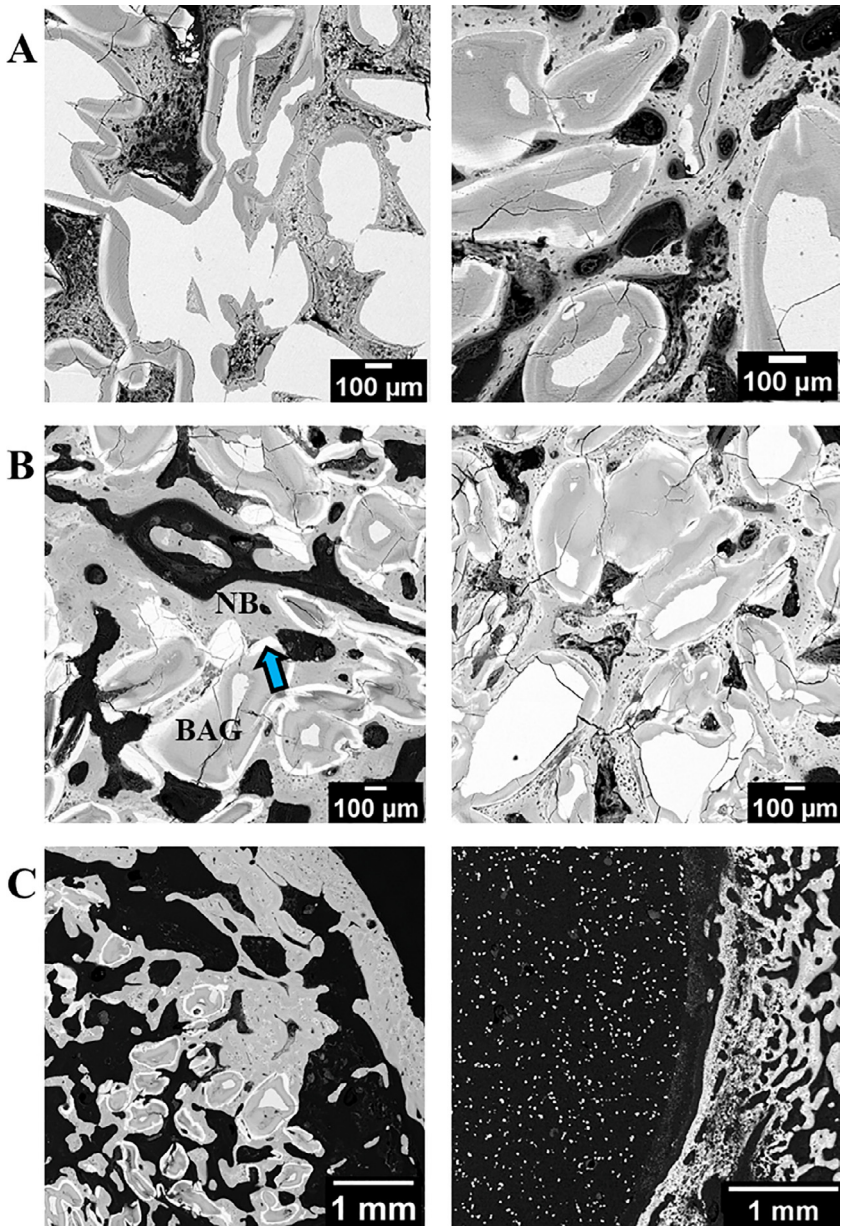

Fig. 6. SEM backscattered electron images of implanted BAG-S53P4 scaffolds. A: Representative close-up SEM images of the center area in BAG-S53P4 scaffolds at 2 (left) and 4 (right) weeks postoperative. Remaining BAG-S53P4 is visible as white, dense areas. Reaction surfaces are visible as grey areas with lighter peripheral rims partly covering the remaining BAG-S53P4 and merging into formed new woven bone inside the porous scaffold. Medullary spaces are visible as black areas. B: Corresponding SEM close-ups from the center area in two BAG-S53P4 scaffolds at 8 weeks postoperative. BAG-S53P4 (BAG), new bone (NB), and reaction surface (arrow) has been labeled in the left image to aid interpretation. C: Representative close-up SEM image of the transversal interface region where bony callus formed around the defect meets an implanted BAG-S53P4 scaffold (left) and a PMMA spacer (right) at 8 weeks postoperative.

bone. There was a close compositional relationship between the CaP layer and newly formed bone.

3.5. Histological assessment of BAG-S53P4 scaffolds

3.5.1. Osteoid and woven bone form inside the BAG-S53P4 scaffolds

BAG-S53P4 scaffold samples stained with Goldner's Masson trichrome stain confirmed the formation of osteoid and mineralization inside the scaffolds already at 2 weeks postoperative, and woven bone of various magnitude at 4 and 8 weeks (Fig. 8).

At 2 weeks, reactive periosteum with ample vascularization was infiltrating the scaffolds, and osteoblasts as well as foci of osteoid and mineralization were found on the internal scaffold surfaces. At 4 weeks, scaffolds contained capillaries and marked woven bone formation enclosing the remaining BAG-S53P4. Focis of intramembranous ossification were found in the scaffolds, and endochondral ossification was observed in areas with possible callus extensions from reactive periosteum. New bone formed a bony network inside the porous scaffold. At 8 weeks, analyzable sections contained abundant vascularization and minor but assessable woven bone formation with accumulation of osteoid and calcified matrix, as well as osteoblasts and osteoclasts on the glass surfaces. Samples also demonstrated progressive maturation of external callus that integrated the scaffolds from 2 to 8 weeks postoperative. Soft, ossifying callus was present at 2 weeks, and periosteal hard callus at 4 weeks. At 8 weeks, samples presented remodeling hard callus containing compact bone and integrating trabeculae with vascularization and active intramembranous ossification.

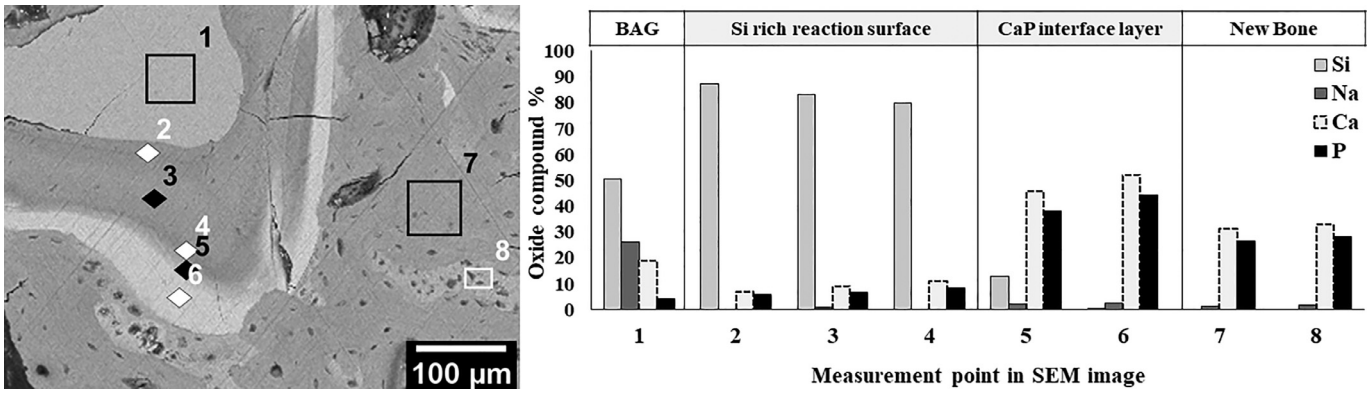

Fig. 7. Representative energy-dispersive X-ray analysis of reaction surface and newly formed bone inside an 8-week BAG-S53P4 scaffold. Si, Na, Ca, and P levels (expressed as oxide compound in percent) for each measuring point (numbered as 1–8 in the SEM image to the left, and in the X-axis in the bar graph to the right) demonstrates the compositional continuum of the reaction surface. The reaction surface consists of a region rich in Si (measuring point 2–4) directly on the surface of remaining BAG-S53P4 (1) and a CaP interface region (5–6) bridging into new woven bone (7–8) formed in the porous scaffold spaces. To aid interpretation, vertical lines in the graph separate the different areas from which the measuring points were obtained.

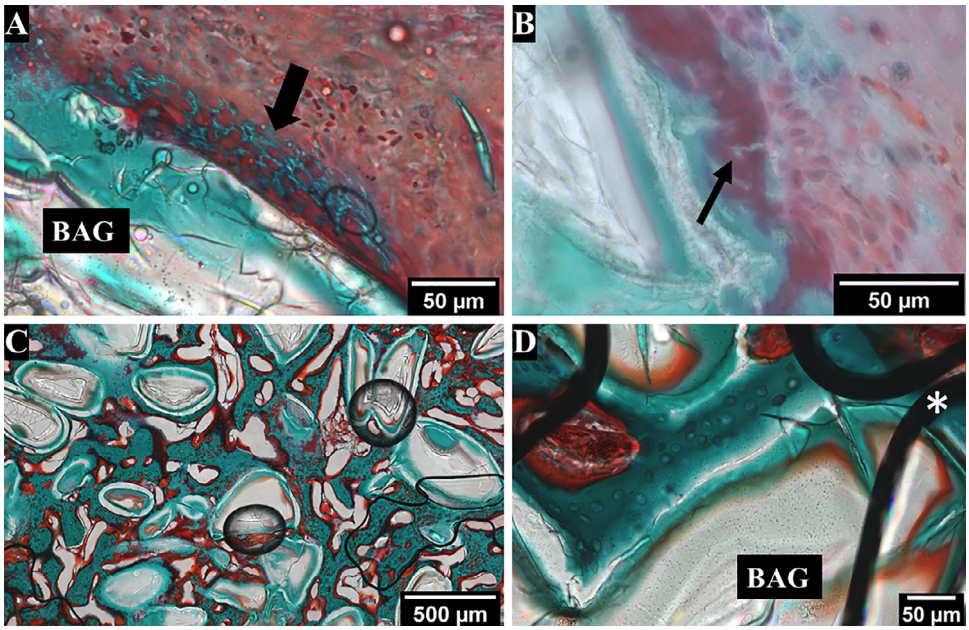

Fig. 8. Close-up images of transversally cut BAG-S53P4 scaffolds stained with Goldner's Masson trichrome stain at 2 (A–B), 4 (C), and 8 (D) weeks postoperative. New bone is stained blue-green, indicated by a bolded arrow in A, and osteoid is stained red-orange, indicated by a thin arrow in B. Osteoblasts are visible as cells in close proximity to the osteoid in B. Remaining BAG-S53P4 (white bright areas, BAG) and one large obscuring air bubble (white asterisk *) has been marked in the 8-week sample (D) to aid interpretation. Note the layered reaction surface on the remaining BAG-S53P4 in all included images (A–D). (For interpretation of the references to color in this figure legend, the reader is referred to the web version of this article.)

Unfortunately, sample preparation difficulties and air-bubble formation restricted the assessment.

3.6. µCT imaging and area measurement analysis of BAG-S53P4 scaffolds

3.6.1. Osseointegration of BAG-S53P4 scaffolds progress markedly from 2 to 8 weeks

Inspection of osseointegrational development in the µCT scans of the resected femur samples exhibited progressive osseointegration of the implanted BAG-S53P4 scaffolds in diaphysis ends and surrounding callus from 2 to 8 weeks. The integration of callus and defect-filling scaffold presented still incomplete but evident early defect bridging at 4 and 8 weeks (Fig. 9).

Osseointegration was progressing in both ends and the middle of the BAG-S53P4 scaffolds during follow-up. However, result homogeneity was highly dependent on the performance of the surgical fixation in keeping the scaffolds in place in the defects and in stable contact with the ends of the diaphysis.

3.6.2. BAG-S53P4 decreases as reaction surface and new bone increases in the scaffolds

Analysis of internal BAG-S53P4 scaffold area measurements demonstrated a significant and constant increase in new bone and reaction surface inside the scaffolds from 2 to 8 weeks (mean percent of total transverse scaffold area: 33.2 ± 1.9% vs. 46.1 ± 1.5%, $p = 0.010$), with a concurrent significant decrease in remaining glass (35.8 ± 3.9% vs. 10.4 ± 1.1%, $p = 0.002$) (Fig. 10). Early development during 2 to 4 weeks was similar, with a notable but not significant increase in new bone and reaction surface (33.2 ± 1.9% vs. 40.4 ± 2.6%), and a significant decrease in remaining glass (35.8 ± 3.9% vs. 21.2 ± 3.2%, $p = 0.031$).

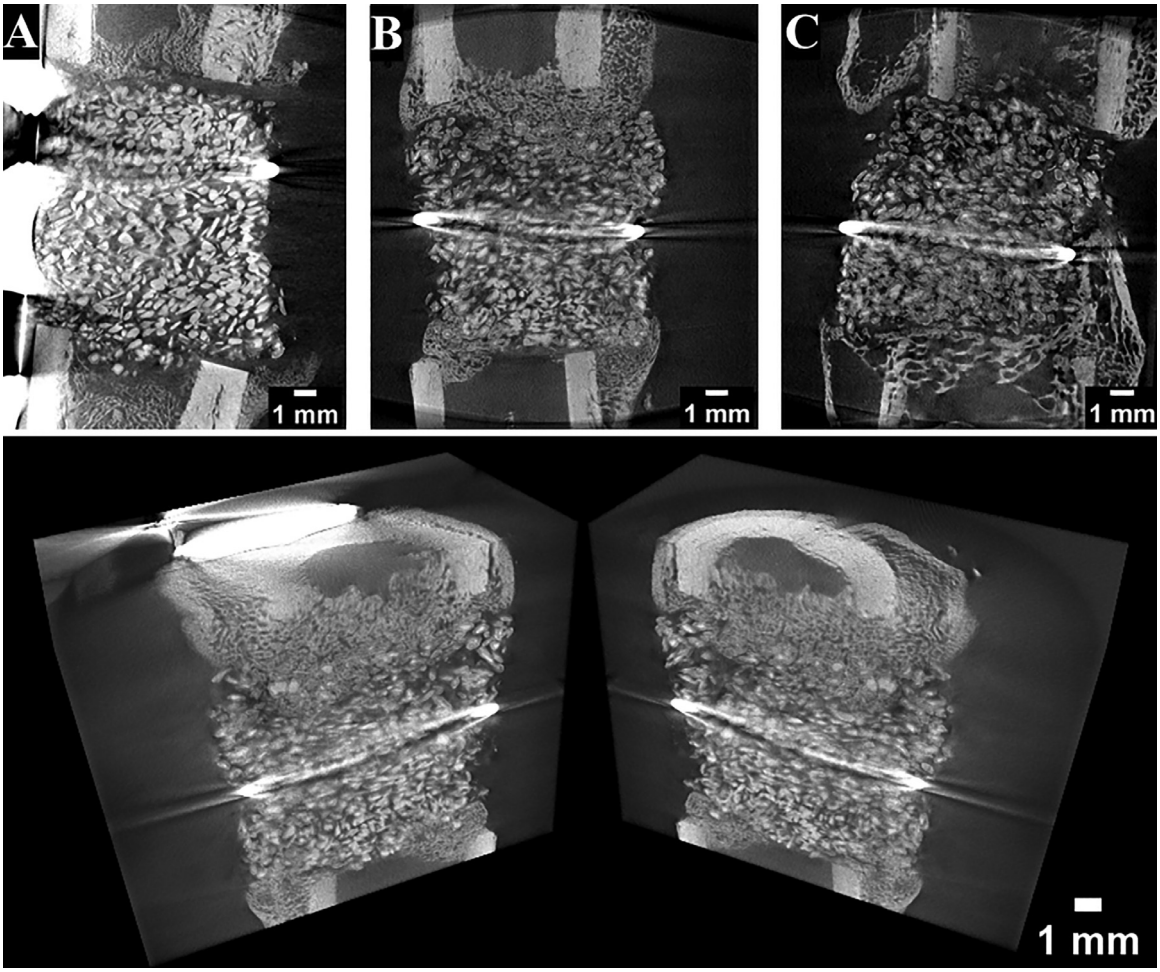

Fig. 9. µCT scans of resected femur samples with implanted BAG-S53P4 scaffolds. Upper row: BAG-S53P4 scaffolds at 2 (A), 4 (B), and 8 (C) weeks postoperative. Lower row: µCT 3D-projection of the same 4-week BAG-S53P4 scaffold as in B in the upper row.

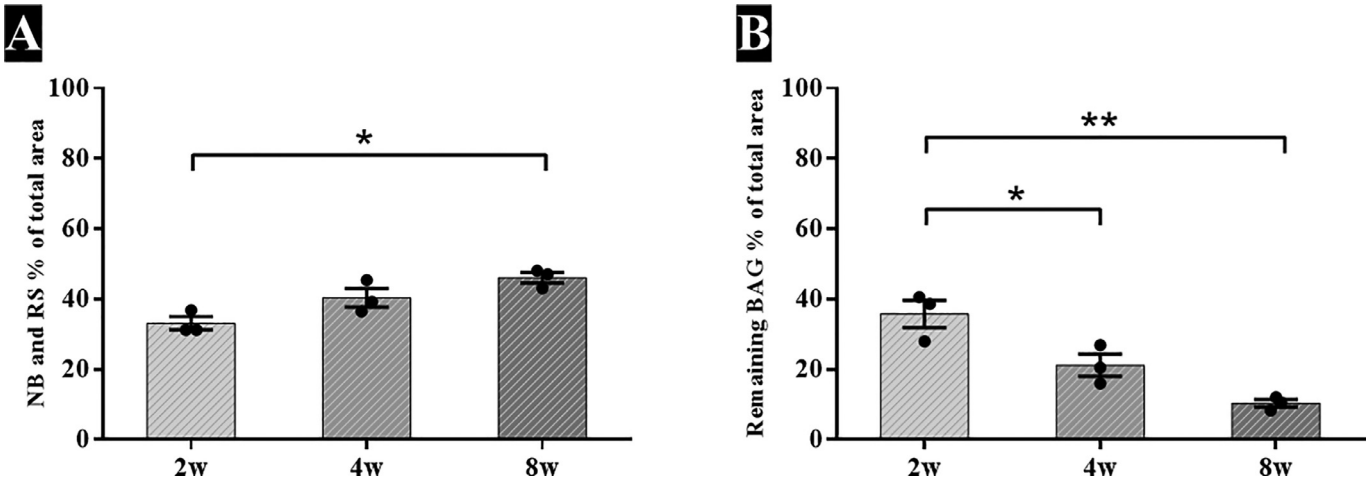

Fig. 10. Analysis of area measurements obtained from µCT images of BAG-S53P4 scaffolds at 2, 4, and 8 weeks postoperative. A: Formation of new bone (NB) and reaction surface (RS) inside the scaffolds. B: Remaining BAG-S53P4 inside the scaffolds. Bars show mean percent (%) of the total transversal scaffold area ± SEM. * indicates a difference for which $p < 0.05$, and ** indicates a difference for which $p < 0.01$.

3.6.3. Reaction surface and new bone forms evenly throughout the BAG-S53P4 scaffolds

Comparative analysis of area measurements of new bone and reaction surface in different regions of the BAG-S53P4 scaffolds revealed that the formation appeared to progress similarly throughout the scaffolds during the 8-week follow-up (Fig. 11). During week 2 to 8, the mean percent of the total transversal scaffold area occupied by new bone and reaction surface increased from 33.2 ± 0.6% to 46.9 ± 0.1% in the end regions, and from 32.8 ± 0.8% to 45.2 ± 1.2% in the middle region. No significant differences were found, and these results were consistent in the

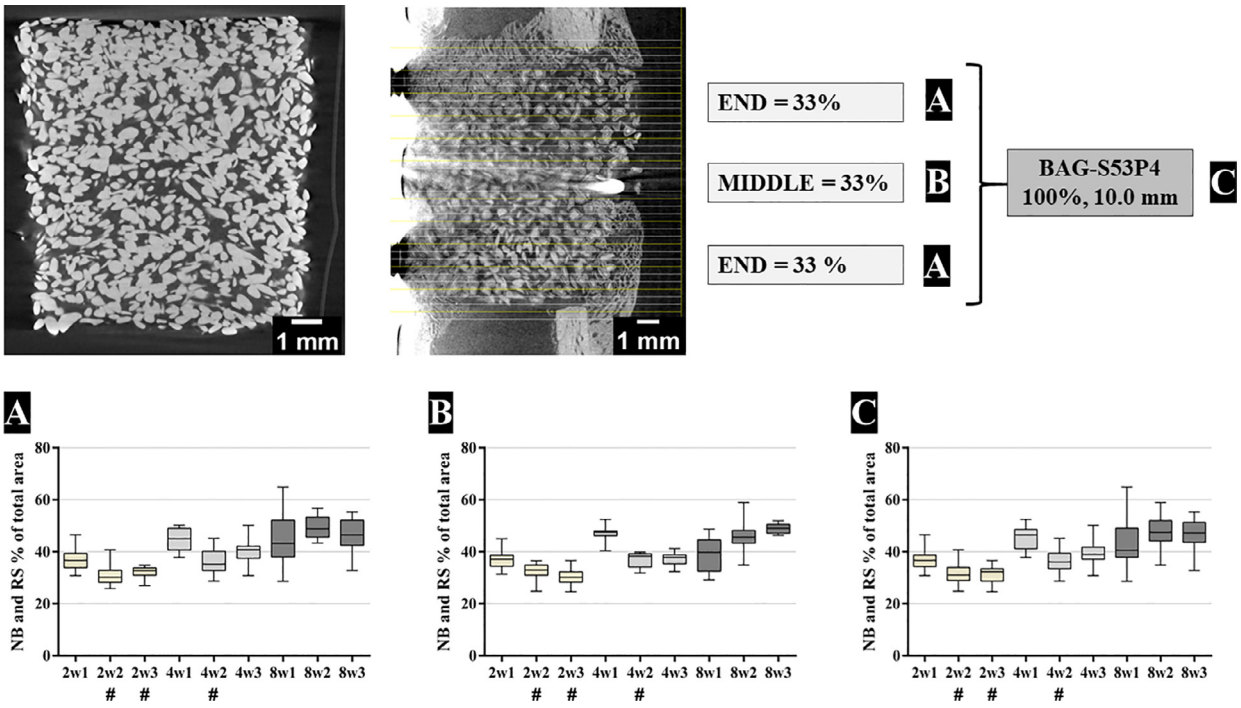

Fig. 11. Formation of new bone and reaction surface in different regions of the BAG-S53P4 scaffolds from 2 to 8 weeks. Upper row: µCT images of an unused (not implanted) BAG-S53P4 scaffold (left) and an implanted 4-week BAG-S53P4 scaffold after femur resection (middle) along with a schematic overview of the regional segmentation for comparison of area measurement data in different scaffold regions (right). Lower row: Formation of new bone (NB) and reaction surface (RS) in the (distal and proximal) end regions (A), middle region (B), and in the whole scaffold (C) at 2, 4, and 8 weeks. The X axis presents the 9 implanted BAG-S53P4 scaffolds included in this study. For example, "2w1" indicates 2-week study endpoint, individual sample one. # below the X axis indicates individual scaffolds that detached during or after resection. Box plots are shown with min. and max values and consist of the area measurements values obtained from the µCT images created from each individual sample.

comparative analysis of remaining BAG-S53P4 in the different scaffold regions.

3.6.4. BAG-S53P4 scaffolds demonstrate intact integrity throughout follow-up

µCT imaging showed no major structural damages in the implanted BAG-S53P4 scaffolds during follow-up but revealed that the fixation wire protruded slightly into the 4- and 8-week scaffolds (Fig. 5).

4. Discussion

This preclinical study evaluated sintered BAG-S53P4 scaffolds *in vivo* in a single-staged, one-implant IM technique for the treatment of critical-sized diaphyseal defects. In this one-implant technique, an amorphous porous BAG-S53P4 scaffold substitutes both the membrane-inducing PMMA spacer and subsequent graft-filling in Masquelet's original two-staged technique. We demonstrated that our BAG-S53P4 scaffolds fulfill prerequisite characteristics of the proposed single-staged IM technique, as they produce BMP-expressing IMs and osseointegrative new bone formation that anchors the scaffolds in surrounding bone. Furthermore, at 8 weeks postoperative all defects presented marked integration of the implanted BAG-S53P4 scaffolds as well as aligned early defect union.

Our study found that BAG-S53P4 scaffolds do indeed produce IMs structurally similar to those of standard PMMA. The IMs were found to be bioactive, with upregulated expressions of the potent osteogenic growth factors BMP-2, BMP-4, and BMP-7. BMPs link osteogenesis to angiogenesis through stimulation of osteoblasts' VEGF-A expression [50], and combined expression of different BMPs has been proposed to provide synergistic benefits [17]. Although clinical studies characterizing gene expressions in human IMs are scarce, previous studies have reported upregulated expressions of BMP-2 and BMP-7 in human PMMA IMs in tibial and femoral segmental defects [51], thus indicating the importance of these BMPs in IM evaluations.

Our results presented upregulated expressions of BMP-2, BMP-4, and BMP-7 in BAG-S53P4 IMs throughout the 8-week follow-up, with peak expressions of the same magnitude as in PMMA IMs. Interestingly, BAG-S53P4 IMs had earlier peak expressions than PMMA IMs. This pattern was not unambiguously statistically significant, but it indicates that BAG-S53P4 affects BMP expressions differently than PMMA – an intriguing finding. In BAG-S53P4 IMs, peak expression of BMP-2 arrived already at 2 weeks, with a subsequent decrease at 4–8 weeks. In contrast, the BMP-2 expression in PMMA IMs was low at 2 weeks and peaked at 4–8 weeks. Expression of BMP-4 in BAG-S53P4 IMs was high at 2–4 weeks, while BMP-4 in PMMA IMs was high at 4 weeks and notably lower at 2 and 8 weeks. Perhaps the most striking result was the near-opposite BMP-7 expression pattern when comparing IMs by BAG-S53P4 and PMMA. These differing patterns is an intriguing find connected to the timing of optimal or mature osteogenic stimulation provided by the IM. In the two-staged IM technique, mature osteogenic stimulation by the PMMA IM is considered to occur around 6–8 weeks after the first surgery. This is in agreement with our results. As PMMA is not a bone substitute, the osteogenic effect provided by the IM will promote defect healing only after the PMMA spacer has been replaced by bone graft. The second surgery, in which bone graft replaces the spacer, should be performed when the PMMA IM has reached its mature osteogenic effect [9–13]. Hence, the actual effect of the IM on defect healing will begin 6–8 weeks after the first surgery. In contrast, BAG-S53P4 is a bone substitute and the BAG-S53P4 scaffold is continuously replaced by new bone from the time of implantation, with no need for a second surgery or bone graft. Early peak expressions in the BAG-S53P4 IMs indicate an early maturation of the osteogenic effect, which promotes defect healing already from 2 weeks postoperative.

The osteogenic effect provided by the BAG-S53P4 IM also appears well-timed when compared with the natural fracture healing process. Similar to BAG-S53P4 IMs, natural fracture healing includes an early peak BMP-2 expression during the first days to weeks to accommodate the high need for mesenchymal stem cells that can differentiate into osteoprogenitor cells, and later peak expressions of BMP-4 and BMP-7 to stimulate further bone formation, soft callus mineralization, and maturation of woven bone and bony callus [52]. As critical-sized diaphyseal defects include several factors that undermine the natural fracture healing process, this timely osteogenic effect provided by the IM might offer added benefits through natural healing enhancement.

To our knowledge, this is the first probative description of osteogenic membranes induced by sintered amorphous BAG-S53P4 scaffolds in critical-sized defects in the femur diaphysis. Previous work by Björkenheim et al. [37] study IMs of non-amorphous BAG-S53P4 scaffolds in a non-critical defect in the femur metaphysis of NZW rabbits. When comparing our findings with the results reported by Björkenheim et al. [37], both differences and similarities emerge. Both defect models show high BMP-2 expression early in the fracture healing process, and lower BMP-2 expressions at 4 and 8 weeks. Expressions of BMP-4 differs, however, as non-critical metaphyseal defects had a low expression at 2 weeks, while our critical-sized diaphyseal model had high expressions throughout 2–4 weeks. When comparing BAG-S53P4 IMs with IMs of PMMA spacers, Björkenheim et al. [37] found that both implants had similar BMP-7 expression patterns during follow-up. This contrasts the inverse BMP-7 expression pattern we found in critical-sized diaphyseal defects.

Dissimilar BMP-expressions at different defect sites are not a surprising find, as there are known differences in the healing of defects in the cancellous metaphysis and cortical diaphysis. The metaphysis is inherently rich in mesenchymal stem cells, with inflammatory cells and stem cells arriving at the defect site simultaneously during healing-initiation. In cortical diaphyseal defects, inflammatory cells precede the stem cells [53–55]. Characterization of the fracture-healing cascades in different parts of the femur is an important part of fracture-healing optimization.

Bioactive IMs with upregulated key BMP expressions strongly indicate osteostimulative effects. Nonetheless, to be clinically useful the BAG-S53P4 scaffolds need to demonstrate formation of new bone. To be considered osteoconductive, a prerequisite for osseointegration, new bone must also grow on the internal surfaces of the scaffold. In this study, we confirmed osteoconductive new bone formation inside the BAG-S53P4 scaffolds. Minor deposits of osteoid and new bone were observed at 2 weeks and progressed to marked amounts of woven bone at 4 and 8 weeks postoperative. Observations were conclusive in SEM and µCT imaging, and, despite limited analyzable samples, also evident in histological assessments.

EDXA confirmed development of the BAG-characteristic bone-bonding CaP layer in the scaffolds. This layer had a close compositional relationship with the new bone, establishing a tight anchorage. As a natural consequence of this anchorage, the separation of new bone and reaction surface was obstructed. Remaining BAG-S53P4 could be clearly detected, however, thus enabling comparison of remaining glass with new bone and reaction surface. Herein, a substitution of BAG-S53P4 into reaction surface and new bone emerged. During the 8-week follow-up, remaining BAG-S53P4 decreased significantly with a concurrent significant increase in new bone and reaction surface. This substitution is key for the mechanical stability of our model. As BAG-S53P4 is biodegradable and thus decreases in volume over time, the combined success of a stable surgical osteosynthesis and transformation of the volume loss into anchoring bone is of particular importance.

This study also presents a more surprising find – the volume of new bone and reaction surface increased in a similar manner in different scaffold regions during the 8-week follow-up. The formation of reaction surface and new bone could be expected to vary in different regions, as the scaffold ends are in direct contact with endogenous bone and bone marrow. This contact would presumably provide essential cells and mediators, in addition to the IM inflow. A conceivable explanation could be attributed to scaffold porosity, as it may be sufficient enough to enable body fluids, cells and osteogenic growth factors to rapidly reach the middle of the scaffolds.

Proof of osteoconductive internal new bone formation further strengthens our hypothesis. However, for sintered BAG-S53P4 scaffolds to be viable in the complex milieu of a large defect in the weight-bearing diaphysis, they also need to demonstrate sufficiently stable osseointegration in surrounding bone. Osseointegration is more durable than osteoconduction and implies that the anchorage between scaffold and bone is retained over time and during functional loading [56]. The implanted scaffold must be able to anchor strongly in the defect through an intergrowth of surrounding bone and the bone forming inside the scaffold, aided by a successful surgical osteosynthesis. This is critical to prevent scaffold detachment during postoperative loading.

In this study, our BAG-S53P4 scaffolds exhibited limited osseointegration at 2 weeks postoperative, clearly indicating that 2 weeks was insufficient to achieve scaffold integration. Indeed, none of the 2-week BAG-S53P4 scaffolds were assessed as fully integrated in the combined manual and X-ray assessment. One 2-week scaffold that was initially assessed as integrated in situ, later dislocated partially after resection – highlighting the importance of the combined support provided by the enclosing tissues and the surgical osteosynthesis during the early postoperative period.

At 4 and 8 weeks, scaffold integration and signs of early defect union had progressed considerably. Bridging integration of the BAG-S53P4 scaffolds into the bony callus and diaphysis ends was clearly observed in both SEM and µCT imaging. Notably, manual and X-ray assessments of 4-week scaffolds rendered heterogenic results, spanning from complete scaffold detachment to a well-integrated scaffold with successful osteosynthesis and early defect union. In contrast, all 8-week BAG-S53P4 scaffolds showed marked integration and all the 8-week defects demonstrated successful osteosynthesis and early union. Thus, this study indicates that 8 postoperative weeks was sufficient time for the BAG-S53P4 scaffolds to achieve homogeneous scaffold integration with early union in a critical-sized segmental defect in the femur diaphysis. In addition, our results suggests that the BAG-S53P4 scaffolds are durable enough for application in these demanding defects. At present, a detailed mechanical scaffold characterization is ongoing and will be published in a later paper.

In terms of limitations, extrapolation of animal studies into humans is always speculative and calls for cautious interpretation. Additionally, our small sample number naturally interferes with statistical generalizability. Nevertheless, this study presents several important considerations for optimizations in future research and modelling.

Our BAG-S53P4 scaffolds were simply cylindrical, while the PMMA spacer used in the original IM technique is shaped to wrap the defect ends. According to Masquelet [57], failure to wrap the ends is a main pitfall of the IM technique that can lead to non-unions. It is indeed observable in some of our samples that while callus and scaffold show evident intergrowth, the callus also protrudes slightly outwards, instead of aligning to the scaffold. We also found that the region where the scaffold meets the end of the diaphysis was the most susceptible to instability interfering with integrative bone formation. Mechanical enhancement of this inter-

face area could be beneficial, for example through development of a BAG-S53P4 scaffold that wraps the defect ends.

The most challenging surgical factor conducting this study, in the authors' experience, was to achieve proper fixation of the BAG-S53P4 scaffold in the defect. A segmental, large defect in the femur diaphysis is weight-bearing and bypasses stabilization from the adjacent fibula, as might benefit a tibial defect model. This enabled our evaluation to focus solemnly on the implanted scaffold in the femur, but it also resulted in inherent instability which requires optimal fixation. Furthermore, while the used defect size has been previously established in NZW rabbits [45], and rabbits are frequent in orthopedic research as their bone mineral density and haversian canals are similar to humans [58,59], they also have strong hind-leg muscles affecting the femur as well as brittle cortices complicating the application of fixation hardware.

The surgical fixation used in our model was a locking compression plate, screws, and a wire. Although we experienced no scaffold breakages and no failures of the plate fixation of the defects, the fixation of the scaffold itself inside the defect was clearly a pitfall. The scaffold fixation has to support the implant during defect loading until the scaffold is integrated and can assist in functional weight-bearing. There are a few alternatives to consider. Veterinary treatments of large femur fractures in NZW rabbits include plates and intramedullary nailing [60,61], a method also used clinically in humans. However, this could limit the evaluation of bone formation as the nail would occupy the scaffold center. Another option used in humans is external fixation, but it is less suited to a preclinical model as it exposes the animals to unnecessary stress. Absorbable mesh wrapping could be considered, but it limits IM examination.

To summarize, a feasible proposal for future research would be an experimental model with larger animals with a femur size and movement pattern more similar to humans. This should be combined with a development of the scaffold to enable a surgical method with a scaffold-integrated intermedullary nail or plate fixation. In any case, optimization of the scaffold fixation is needed to avoid unnecessary instability and evaluate the full potential of these promising BAG-S53P4 scaffolds in large weight-bearing defects, whether in a preclinical or clinical study.

5. Conclusions

This is the first study evaluating the functional potential of amorphous porous BAG-S53P4 scaffolds *in vivo* in critical-sized segmental diaphyseal defects treated with a single-staged version of Masquelets IM technique. The original two-staged IM technique utilizes a PMMA spacer to produce a defect-enclosing IM that forms the basis of the defect healing as it provides osteogenic cells, blood vessels, cytokines and growth factors that support bone formation. When the IM has matured, the PMMA spacer is replaced with bone graft which compensates for the bone loss, and the defect heals. To develop a single-staged IM technique, a single implant that combines the original functions of both the PMMA spacer and the bone graft is needed.

We demonstrated that our BAG-S53P4 scaffolds induce osteostimulative defect-enclosing membranes and achieve stable scaffold integration with early defect union in a large, weight-bearing diaphyseal defect in rabbit femur at 4 to 8 weeks postoperative. These results support the hypothesis that scaffolds sintered from BAG-S53P4 are a suitable bone substitute in a single-stage IM technique for the treatment of critical-sized segmental diaphyseal defects in long bones. Future research is needed to shed light on the full capacity of these scaffolds in an optimized surgical model.

Disclosures

Nina Lindfors is a Clinical advisor for Bonalive Biomaterials.

Declaration of Competing Interest

The authors declare that they have no known competing financial interests or personal relationships that could have appeared to influence the work reported in this paper.

Acknowledgements

We thank Bonalive Biomaterials (Turku, Finland) for kindly providing the BAG-S53P4 granules for this study. We also thank the FIMM Digital Microscopy and Molecular Pathology Unit supported by Helsinki University and Biocenter Finland, BioSiteHisto Ltd., and the Finnish Centre for Laboratory Animal Pathology at the Department of Veterinary Biosciences, Faculty of Veterinary Medicine, University of Helsinki for their assistance in processing, scanning, and providing histological assessment of the BAG-S53P4 scaffold samples. This work was supported by grants provided by the Medical Society of Finland and Helsinki University Hospital.

References

[1] P.V. Giannoudis, I. Pountos, Tissue regeneration, Injury 36 (2005) S2–S5, doi:10.1016/j.injury.2005.10.006.
[2] P.V. Giannoudis, T.A. Einhorn, D. Marsh, Fracture healing: the diamond concept, Injury 38 (2007) S3–S6, doi:10.1016/S0020-1383(08)70003-2.
[3] F. Loi, L.A. Córdova, J. Pajarinen, T. Lin, Z. Yao, S.B. Goodman, Inflammation, fracture and bone repair, Bone 86 (2016) 119–130, doi:10.1016/j.bone.2016.02.020.
[4] E.H. Schemitsch, Size matters: defining critical in bone defect size, J. Orthop. Trauma 31 (2017) S20–S22, doi:10.1097/BOT.0000000000000978.
[5] J.F. Keating, A.H.R.W. Simpson, C.M. Robinson, The management of fractures with bone loss, J. Bone Joint Surg. Br. 87-B (2005) 142–150, doi:10.1302/0301-620X.87B2.15874.
[6] T.J. Blokhuis, Management of traumatic bone defects: metaphyseal versus diaphyseal defects, Injury 48 (2017) S91–S93, doi:10.1016/j.injury.2017.04.021.
[7] G. Marongiu, A. Dolci, M. Verona, A. Capone, The biology and treatment of acute long-bones diaphyseal fractures: overview of the current options for bone healing enhancement, Bone Rep. 12 (2020) 100249, doi:10.1016/j.bonr.2020.100249.
[8] A.C. Masquelet, F. Fitoussi, T. Begue, G.P. Muller, Reconstruction des os longs par membrane induite et autogreffe spongieuse [Reconstruction of the long bones by the induced membrane and spongy autograft], Ann. Chir. Plast. Esthet. 45 (2000) 346–353.
[9] L. Vidal, C. Kampleitner, M.Á. Brennan, A. Hoornaert, P. Layrolle, Reconstruction of large skeletal defects: current clinical therapeutic strategies and future directions using 3D printing, Front. Bioeng. Biotechnol. 8 (2020) 61, doi:10.3389/fbioe.2020.00061.
[10] A.C. Masquelet, T. Kishi, P.E. Benko, Very long-term results of post-traumatic bone defect reconstruction by the induced membrane technique, Orthop. Traumatol.: Surg. Res. 105 (2019) 159–166, doi:10.1016/j.otsr.2018.11.012.
[11] J.-C. Aurégan, T. Bégué, Induced membrane for treatment of critical sized bone defect: a review of experimental and clinical experiences, Int. Orthop. (SICOT) 38 (2014) 1971–1978, doi:10.1007/s00264-014-2422-y.
[12] A. Masquelet, N.K. Kanakaris, L. Obert, P. Stafford, P.V. Giannoudis, Bone repair using the masquelet technique, J. Bone Joint Surg. 101 (2019) 1024–1036, doi:10.2106/JBJS.18.00842.
[13] W. Wang, K.W.K. Yeung, Bone grafts and biomaterials substitutes for bone defect repair: a review, Bioactive Mater. 2 (2017) 224–247, doi:10.1016/j.bioactmat.2017.05.007.
[14] J. Patel, K.P. Gudehithlu, G. Dunea, J.A.L. Arruda, A.K. Singh, Foreign body-induced granulation tissue is a source of adult stem cells, Transl. Res. 155 (2010) 191–199, doi:10.1016/j.trsl.2009.08.010.
[15] P.H. Pelissier, A.C. Masquelet, R. Bareille, S.M. Pelissier, J. Amedee, Induced membranes secrete growth factors including vascular and osteoinductive factors and could stimulate bone regeneration, J. Orthop. Res. 22 (2004) 73–79, doi:10.1016/S0736-0266(03)00165-7.
[16] J.M. Wozney, V. Rosen, A.J. Celeste, L.M. Mitsock, M.L. Whitters, M.J.R.W. Kriz, R.M. Hewick, E.A. Wang, Novel regulators of bone formation: molecular clones and activities, Science 242 (1988) 1528–1534, doi:10.1126/science.3201241.
[17] H. Cheng, W. Jiang, F.M. Phillips, R.C. Haydon, Y. Peng, L. Zhou, H.H. Luu, N. An, B. Breyer, P. Vanichakarn, J.P. Szatkowski, J.Y. Park, T.-C. He, Osteogenic activity of the fourteen types of human bone morphogenetic proteins (BMPs), J. Bone Joint Surg.-Am. 85 (2003) 1544–1552, doi:10.2106/00004623-200308000-00017.

[18] P.V. Giannoudis, T.A. Einhorn, Bone morphogenetic proteins in musculoskeletal medicine, Injury 40 (2009) S1–S3, doi:10.1016/S0020-1383(09)00642-1.
[19] G.M. Calori, P.V. Giannoudis, Enhancement of fracture healing with the diamond concept: the role of the biological chamber, Injury 42 (2011) 1191–1193, doi:10.1016/j.injury.2011.04.016.
[20] P.V. Giannoudis, P.J. Harwood, T. Tosounidis, N.K. Kanakaris, Restoration of long bone defects treated with the induced membrane technique: protocol and outcomes, Injury 47 (2016) S53–S61, doi:10.1016/S0020-1383(16)30840-3.
[21] A. Moghaddam, B. Thaler, T. Bruckner, M. Tanner, G. Schmidmaier, Treatment of atrophic femoral non-unions according to the diamond concept: results of one- and two-step surgical procedure, J. Orthop. 14 (2017) 123–133, doi:10.1016/j.jor.2016.10.003.
[22] T.F. Raven, A. Moghaddam, C. Ermisch, F. Westhauser, R. Heller, T. Bruckner, G. Schmidmaier, Use of Masquelet technique in treatment of septic and atrophic fracture nonunion, Injury 50 (2019) 40–54, doi:10.1016/j.injury.2019.06.018.
[23] A. Oryan, S. Alidadi, A. Moshiri, N. Maffulli, Bone regenerative medicine: classic options, novel strategies, and future directions, J. Orthop. Surg. Res. 9 (2014) 18, doi:10.1186/1749-799X-9-18.
[24] L.L. Hench, The story of Bioglass®, J. Mater. Sci.: Mater. Med. 17 (2006) 967–978, doi:10.1007/s10856-006-0432-z.
[25] L.L. Hench, H.A. Paschall, Direct chemical bond of bioactive glass-ceramic materials to bone and muscle, J. Biomed. Mater. Res. 7 (1973) 25–42, doi:10.1002/jbm.820070304.
[26] A.M. Gatti, G. Valdrè, Ö.H. Andersson, Analysis of the in vivo reactions of a bioactive glass in soft and hard tissue, Biomaterials 15 (1994) 208–212, doi:10.1016/0142-9612(94)90069-8.
[27] P. Virolainen, J. Heikkilä, A. Yli-Urpo, E. Vuorio, H.T. Aro, Histomorphometric and molecular biologic comparison of bioactive glass granules and autogenous bone grafts in augmentation of bone defect healing, J. Biomed. Mater. Res. 35 (1997) 9–17, doi:10.1002/(sici)1097-4636(199704)35:1⟨9::aid-jbm2⟩3.0.co;2-s.
[28] V.-V. Välimäki, H.T. Aro, Molecular basis for action of bioactive glasses as bone graft substitute, Scand. J. Surg. 95 (2006) 95–102, doi:10.1177/145749690609500204.
[29] A. Hoppe, N.S. Güldal, A.R. Boccaccini, A review of the biological response to ionic dissolution products from bioactive glasses and glass-ceramics, Biomaterials 32 (2011) 2757–2774, doi:10.1016/j.biomaterials.2011.01.004.
[30] E. Munukka, O. Leppäranta, M. Korkeamäki, M. Vaahtio, T. Peltola, D. Zhang, L. Hupa, H. Ylänen, J.I. Salonen, M.K. Viljanen, E. Eerola, Bactericidal effects of bioactive glasses on clinically important aerobic bacteria, J. Mater. Sci.: Mater. Med. 19 (2008) 27–32, doi:10.1007/s10856-007-3143-1.
[31] J.S. Fernandes, P. Gentile, R.A. Pires, R.L. Reis, P.V. Hatton, Multifunctional bioactive glass and glass-ceramic biomaterials with antibacterial properties for repair and regeneration of bone tissue, Acta Biomater. 59 (2017) 2–11, doi:10.1016/j.actbio.2017.06.046.
[32] N.A.P. van Gestel, J. Geurts, D.J.W. Hulsen, B. van Rietbergen, S. Hofmann, J.J. Arts, Clinical applications of S53P4 bioactive glass in bone healing and osteomyelitic treatment: a literature review, Biomed. Res. Int. 2015 (2015) 1–12, doi:10.1155/2015/684826.
[33] I. Gergely, Ö. Nagy, Zagyva Ancuţa, S. Gy. Zuh, O.M. Russu, Our short-term experience with the use of S53P4 (BonAlive®) bioactive glass as a bone graft substitute, Acta Medica Marisiensis 57 (2011) 627–630.
[34] N.C. Lindfors, I. Koski, J.T. Heikkilä, K. Mattila, A.J. Aho, A prospective randomized 14-year follow-up study of bioactive glass and autogenous bone as bone graft substitutes in benign bone tumors, J. Biomed. Mater. Res. 9999B (2010) NA-NA, doi:10.1002/jbm.b.31636.
[35] M.C. Tanner, R. Heller, F. Westhauser, M. Miska, T. Ferbert, C. Fischer, S. Gantz, G. Schmidmaier, P. Haubruck, Evaluation of the clinical effectiveness of bioactive glass (S53P4) in the treatment of non-unions of the tibia and femur: study protocol of a randomized controlled non-inferiority trial, Trials 19 (2018) 299, doi:10.1186/s13063-018-2681-9.
[36] R. Björkenheim, G. Strömberg, J. Pajarinen, M. Ainola, P. Uppstu, L. Hupa, T.O. Böhling, N.C. Lindfors, Polymer-coated bioactive glass S53P4 increases VEGF and TNF expression in an induced membrane model in vivo, J. Mater. Sci. 52 (2017) 9055–9065, doi:10.1007/s10853-017-0839-6.
[37] R. Björkenheim, G. Strömberg, M. Ainola, P. Uppstu, L. Aalto-Setälä, L. Hupa, J. Pajarinen, N.C. Lindfors, Bone morphogenic protein expression and bone formation are induced by bioactive glass S53P4 scaffolds in vivo, J. Biomed. Mater. Res. 107 (2019) 847–857, doi:10.1002/jbm.b.34181.
[38] J.R. Jones, Reprint of: review of bioactive glass: from hench to hybrids, Acta Biomater. 23 (2015) S53–S82, doi:10.1016/j.actbio.2015.07.019.
[39] J. Massera, L. Hupa, Influence of SrO substitution for CaO on the properties of bioactive glass S53P4, J. Mater. Sci.: Mater. Med. 25 (2014) 657–668, doi:10.1007/s10856-013-5120-1.
[40] L. Aalto-Setälä, P. Uppstu, P. Sinytsyna, N.C. Lindfors, L. Hupa, Amorphous S53P4 glass scaffolds for in vivo applications, Manuscript in preparation. (2020).
[41] S. Fagerlund, J. Massera, N. Moritz, L. Hupa, M. Hupa, Phase composition and in vitro bioactivity of porous implants made of bioactive glass S53P4, Acta Biomater. 8 (2012) 2331–2339, doi:10.1016/j.actbio.2012.03.011.
[42] Editor(s): J. Heikkilä, 8 - Use of bioactive glasses as bone substitutes in orthopaedics and traumatology, in: Heimo O. Ylänen (Ed.), Woodhead Publishing Series in Biomaterials, Bioactive Glasses, Woodhead Publishing, 2011, pp. 189–208. ISBN 9781845697686.
[43] C.-Y. Lin, Y.-H. Chang, K.-J. Lin, T.-C. Yen, C.-L. Tai, C.-Y. Chen, W.-H. Lo, I.-T. Hsiao, Y.-C. Hu, The healing of critical-sized femoral segmental bone defects in rabbits using baculovirus-engineered mesenchymal stem cells, Biomaterials 31 (2010) 3222–3230, doi:10.1016/j.biomaterials.2010.01.030.
[44] K.-T. Peng, M.-Y. Hsieh, C.T. Lin, C.-F. Chen, M.S. Lee, Y.-Y. Huang, P.-J. Chang, Treatment of critically sized femoral defects with recombinant BMP-2 delivered by a modified mPEG-PLGA biodegradable thermosensitive hydrogel, BMC Musculoskelet Disord. 17 (2016) 286, doi:10.1186/s12891-016-1131-7.
[45] M.J. Concannon, M.T. Boschert, C.L. Puckett, Bone induction using demineralized bone in the rabbit femur: a long-term study, Plast. Reconstr. Surg. 99 (June (7)) (1997) 1983–1988, doi:10.1097/00006534-199706000-00025.
[46] T.D. Schmittgen, K.J. Livak, Analyzing real-time PCR data by the comparative C(T) method, Nat. Protoc. 3 (2008) 1101–1108, doi:10.1038/nprot.2008.73.
[47] M.L. McHugh, Multiple comparison analysis testing in ANOVA, Biochem. Med. (2011) 203–209, doi:10.11613/BM.2011.029.
[48] A. Hazra, N. Gogtay, Biostatistics series module 3: comparing groups: numerical variables, Indian J. Dermatol. 61 (2016) 251, doi:10.4103/0019-5154.182416.
[49] K. Rani Das, A brief review of tests for normality, AJTAS 5 (2016) 5, doi:10.11648/j.ajtas.20160501.12.
[50] M.M.L. Deckers, R.L.V. Bezooijen, J. Hoogendam, Bone morphogenetic proteins stimulate angiogenesis through osteoblast-derived vascular endothelial growth factor A, Endocrinology 143 (2002) 1545–1553, doi:10.1210/endo.143.4.8719.
[51] H.E. Gruber, G. Ode, J. Ingram, S. Bethea, M.J. Bosse, Osteogenic, stem cell and molecular characterisation of the human induced membrane from extremity bone defects, Bone Joint Res. 5 (2016) 106–115, doi:10.1302/2046-3758.54.2000483.
[52] M. Bernhardsson, P. Aspenberg, Osteoblast precursors and inflammatory cells arrive simultaneously to sites of a trabecular-bone injury, Acta Orthopaedica 89 (2018) 457–461, doi:10.1080/17453674.2018.1481682.
[53] T. Ono, H. Takayanagi, Osteoimmunology in bone fracture healing, Curr. Osteoporos. Rep. 15 (2017) 367–375, doi:10.1007/s11914-017-0381-0.
[54] K. Kumagai, A. Vasanji, J.A. Drazba, R.S. Butler, G.F. Muschler, Circulating cells with osteogenic potential are physiologically mobilized into the fracture healing site in the parabiotic mice model, J. Orthop. Res. 26 (2008) 165–175, doi:10.1002/jor.20477.
[55] R. Dimitriou, E. Tsiridis, P.V. Giannoudis, Current concepts of molecular aspects of bone healing, Injury 36 (2005) 1392–1404, doi:10.1016/j.injury.2005.07.019.
[56] T. Albrektsson, C. Johansson, Osteoinduction, osteoconduction and osseointegration, Eur. Spine J. 10 (2001) 96–101, doi:10.1007/s005860100282.
[57] A.C. Masquelet, Induced membrane technique: pearls and pitfalls, J. Orthop. Trauma 31 (2017) 36–38, doi:10.1097/BOT.0000000000000979.
[58] A. Schafrum Macedo, C. Cezaretti Feitosa, F. Yoiti Kitamura Kawamoto, P. Vinicius Tertuliano Marinho, Í.dos Santos Dal-Bó, B. Fiuza Monteiro, L. Prado, T. Bregadioli, G. Antonio Covino Diamante, C. Ricardo Auada Ferrigno, Animal modeling in bone research—should we follow the white rabbit? Anim. Models Exp. Med. 2 (2019) 162–168, doi:10.1002/ame2.12083.
[59] Y. Li, S.-K. Chen, L. Li, L. Qin, X.-L. Wang, Y.-X. Lai, Bone defect animal models for testing efficacy of bone substitute biomaterials, J. Orthop. Transl. 3 (2015) 95–104, doi:10.1016/j.jot.2015.05.002.
[60] J.D. Reuter, S. Ovadia, P. Howell, D.H. Jaskwich, Femoral fracture repair and postoperative management in New Zealand white rabbits, Contemp. Top. Lab. Anim. Sci. 41 (2002) 49–52 PMID: 12109898.
[61] M. Crigel, M. Balligand, Critical size defect model on the femur in rabbits, Vet. Compart. Orthop. Traumatol. 15 (2002) 158–163, doi:10.1055/s-0038-1632731.